

Three-Dimensional Imaging of Hidden Objects Using Positron Emission Backscatter

Dongwon Lee, Misa Cowee, Ed Fenimore, Mark Galassi, Quinn Looker, Wendy Vogan-McNeil, Laura Stonehill, Mark Wallace

Los Alamos National Laboratory, Los Alamos, NM 87545 USA

Abstract—Positron emission backscatter imaging is a technique for interrogation and three-dimensional (3-D) reconstruction of hidden objects when we only have access to the objects from one side. Using time-of-flight differences in detected direct and backscattered positron-emitted photons, we construct 3-D images of target objects. Recently at Los Alamos National Laboratory, a fully three-dimensional imaging system has been built and the experimental results are discussed in this paper. Quantitative analysis of images reconstructed in both two- and three-dimensions are also presented.

I. INTRODUCTION

The goal of the backscatter imaging project is to produce a laboratory instrument that forms 3-D images of objects of interest in concealed configurations to which we have access from only one side. This method interrogates a scene by generating a flux of gamma rays from a positron-emitting radioactive source, ^{68}Ge . The positrons emitted by the source decay into two photons which have identical energy of 511 keV and almost opposite directions. Fig. 1 shows a schematic view of this technique. The positron source is placed at the origin and two 511 keV gamma-rays are emitted in opposite directions. The direct photon hits the position-sensitive detector while the backscatter photon hits the object of interest, scatters according to the Compton formula, and then hits one of backscatter detectors. From the recorded positions, energies, and times of the two gamma-ray hits, the 3-D location of the scattering in the object of interest can be reconstructed. Previous works have successfully demonstrated 1-D and 2-D imaging results based on backscatter [1]–[3].

In this section the notations in Fig. 1 are referred to and time-of-flight (TOF) information is used to calculate $\vec{x}_s(x_s, y_s, z_s)$. The positron-emitting source is placed at the origin, and the locations of the detectors where the direct and backscattered photons are observed give us \vec{x}_0 and \vec{x}_1 . The times t_0 and t_1 are obtained at which the measurements \vec{x}_0 and \vec{x}_1 were made, and hence the time difference Δt can be calculated. Photon 0 travels distance of $|\vec{x}_0|$ while photon 1

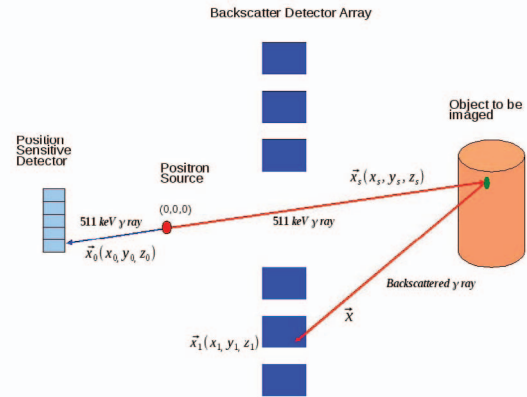


Fig. 1. General view of a Compton backscatter event. Back-to-back 511 keV gamma-rays are emitted from the positron source at (0,0,0). The direct photon hits the position-sensitive detector (light blue rectangle) while the backscattered photon hits the target object, Compton scatters, and then hits one of the backscatter detectors (dark blue rectangles). Our coordinate system is defined where X is into the plane, Y is up, and Z points in the direction from the source to the target object.

travels $|\vec{x}_s| + |\vec{x}_1 - \vec{x}_s|$. Therefore, the relationship between time difference and hit locations is given by

$$c\Delta t = |\vec{x}_s| + |\vec{x}_1 - \vec{x}_s| - |\vec{x}_0|, \quad (1)$$

where c is speed of light. In addition, the relationship between $|\vec{x}_1|$ and $|\vec{x}_s|$ is given by

$$|\vec{x}_1 - \vec{x}_s|^2 = |\vec{x}_1|^2 + |\vec{x}_s|^2 - 2\vec{x}_1 \cdot \vec{x}_s \quad (2)$$

Because the two gamma rays are emitted back-to-back, \vec{x}_s is directly related to \vec{x}_0 as follows.

$$\vec{x}_s = a\vec{x}_0, \quad (3)$$

where a is a constant.

Finally, the constant a is expressed in terms of \vec{x}_0 , \vec{x}_1 and Δt after combining all these equations, and given by

$$a = \frac{1}{2} \frac{|\vec{x}_1|^2 - |\vec{x}_0|^2 - 2|\vec{x}_0|c\Delta t - (c\Delta t)^2}{|\vec{x}_0|^2 + |\vec{x}_0|c\Delta t + \vec{x}_1 \cdot \vec{x}_0} \quad (4)$$

Manuscript received November 13, 2009.

Dongwon Lee is with the Los Alamos National Laboratory, Los Alamos, NM 87545 USA (e-mail: dwlee@lanl.gov).

Once position and time information from the direct and backscatter detectors are known, constant a of a Compton backscatter event can be easily calculated from the equation shown above. Then, the coordinate of the scatter point $\vec{x}_s(x_s, y_s, z_s)$ is obtained from Equation (3). Consequently, 3-D images of the objects can be reconstructed as data is accumulated and the scattering location is calculated for each event. The quality of a 3-D image is highly dependent on uncertainties in our measurements, and the reconstructed Z position is especially depending on the time difference Δt . Therefore, it is crucial to obtain high resolution timing spectra for 3-D Compton scatter imaging.

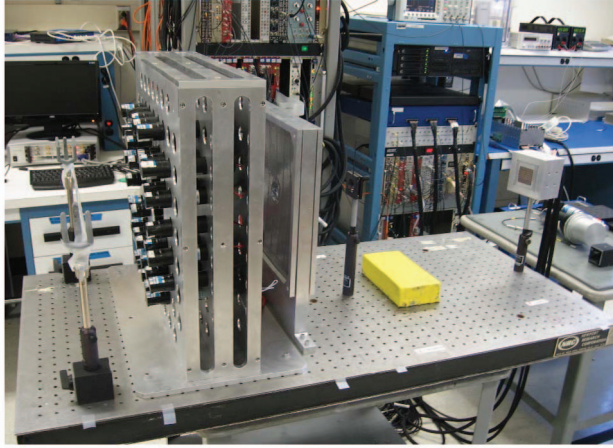


Fig. 2. 3-D laboratory system

II. EXPERIMENTAL SETUP

The laboratory 3-D backscatter system has been configured with a 10x10 pixellated LaBr₃ detector for detection of the direct photons and 32 single LaBr₃ crystals for detection of the backscattered photons. The pixellated LaBr₃ detector was coupled to a Hamamatsu H8500 PMT, which has 8x8 pixels (active area of 49mm x 49mm) each with a separate readout as well as a readout of the last dynode. For the backscattered photon detection, 32 1" single LaBr₃ crystals were mounted on detector holder designed to hold up to 64 detectors. Each single crystal was coupled to a Hamamatsu H6533 PMT for the signal readout. Fig. 2 shows a photograph of the direct detector and the array of the 32 single backscatter detectors used in our laboratory system. We also added a lead shield between the source and the backscatter detector holder in order to prevent the backscattered photons from being directly detected by the backscatter detectors before scattering off the target object. The positions of the direct and the backscatter detectors are scenario-dependent and should be determined after taking into account the desired field-of-view (FOV) and spatial resolution of the object with consideration of the required exposure time and accessible distance of the objects from the detectors.

The electronics for implementing this technique are built around VME-based (Virtual Machine Environment) modules,

and custom-built splitter boxes were used to split input signals into prompt and delayed ones. Prompt signals are used for trigger logic and timing information through TDC (Time-to-digital converter) while delayed signals are integrated in the QDC (Charge-to-digital converter) modules.

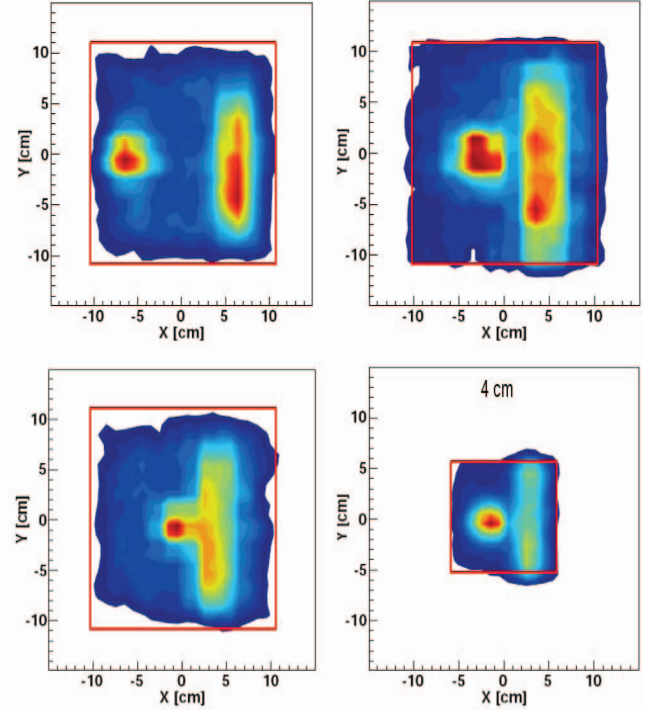


Fig. 3. 2-D images of a copper pipe and a stack of quarters for different separations. All images shown here were reconstructed from experimental data. Red-colored squares represent the field-of-view. The objects are located 60cm from the source in Z-direction, varying separation of two objects in X-direction; Two objects are 12cm apart (top left), 6cm (top right), and 4cm (bottom left), respectively. Image resolution of about 2cm was achieved in all three cases, and we obtained improved image of 4cm separation (bottom right) with 1cm resolution by moving the pixellated detector further away from the source. As a result, two objects are clearly separated with finer image resolution while size of the field-of-view is reduced.

III. RESULTS

Energy resolution for each detector was determined by a series of measurements using several different gamma-ray sources. Typical energy resolution of single LaBr₃ crystal is about 3.25% FWHM at 662keV. Timing resolution was around 233ps FWHM when the time-of-flight difference between two single crystals was measured with two back-to-back 511keV gamma rays. Using several gamma-ray sources, energy calibration for the direct photon detector was performed in similar manner as the backscatter detectors. To test 3-D reconstruction capabilities, as well as the timing calibrations for the 32-backscatter-detector setup, two objects at different z-positions were positioned in the experimental setup; a stack of three quarters (2.5cm diameter by 0.5cm

thick) next to a copper pipe (1cm in diameter) in the xy-plane. For some of the runs a piece of 1/2-inch thick drywall was placed in front of them. The backscatter detectors and the detector holder were located at 44cm from the source.

In order to characterize how well this system can resolve objects in the xy-plane and in the z direction, spatial separation between two metal objects in the xy-plane and spatial separation between the drywall and metal objects in the z direction were varied, respectively. Fig. 3 shows the 2-D reconstructed images of the target objects for varying spatial separations. For these runs, the metal objects were at 60cm from the source. The spatial separation between the quarters and the copper pipe was varied between 4 and 12cm. The backscatter detectors and their holder were at 45cm, and the pixellated direct photon detector was 13cm from the source in the opposite direction. At these distances, the spatial resolution at the metal objects position was about 2cm. For the 12cm and 6cm separations, the two objects were clearly separated in the image, and the different shapes of the images were also clearly visible. For the 4cm separation, the separation was not obvious at these spatial resolutions. If the setup was changed so that the pixellated detector was 25.5cm from the source (i.e. moved it back 12.5cm from its previous position), the spatial resolution at the metal objects' position was improved to 1cm due to decreased ratio between distances from the source to the direct detectors and to the objects. In this case, the two objects were clearly seen as separate in the reconstructed image.

Next, the metal objects are kept at a fixed 4cm separation in the xy-plane while their position in z is varied between 75, 80, and 90cm, and the drywall is at 65cm. The backscatter detectors and holder are at 45cm while the pixellated detector's

position is varied so that the spatial resolution at the metal objects' position will always be 1cm. Fig. 4 shows the image reconstructions along the z direction for events which include the scattering off the drywall. 3-D image of the reconstructed objects are also shown in Fig. 5. Drywall and the metal objects are revealed when 2-D xy slice plane moves along Z-axis as shown in Fig. 5.

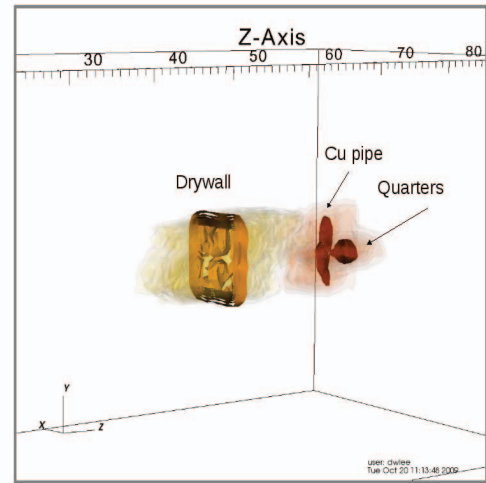


Fig. 5. 3-D image of reconstructed metal objects and drywall from experimental measurement. Drywall and metal objects are clearly shown as 2-D xy slice plane moves along Z-axis.

IV.CONCLUSION

The three-dimensional positron emission backscatter imaging system is built on well-understood Compton scattering and time-of-flight equations [4]-[6] and experimental efforts support the three-dimension imaging capability of the system. These experiment has proved that the Compton backscatter system is able to image objects in 3-D, but the resolution and clarity of the images is ultimately limited by issues related to time difference resolution and our particular direct photon detector. However, 2-D and 3-D imaging capabilities with the full system has been demonstrated successfully.

REFERENCES

- [1] J. R. Tickner et al., "Feasibility study for a low-cost 3-D gamma-ray camera, Appl. Radiation and Isotopes 61 (2004) 67
- [2] J. Gerl et al., "High-resolution gamma backscatter imaging for technical applications", Nucl. Instrum. Meth. A 525 (2004) 328
- [3] Q. Looker et al., "Demonstration of Imaging via Backscattering of Annihilation Gamma Rays", submitted to Nucl. Instrum. Meth. A
- [4] J. Kostamovaara et al., "Distance determination by the gamma-ray time-of-flight method, IEEE Transactions on Instrum. and Meas. 41(5) (1992) 616
- [5] W. W. Moses, "Time of flight in PET revisited, IEEE Trans. Nucl. Sci. 50 (2003) 1325"
- [6] S. Surti et al., "Investigation of Time-of-Flight benefit for fully 3-D PET, IEEE Trans. Med. Imag. 25 (2006) 529

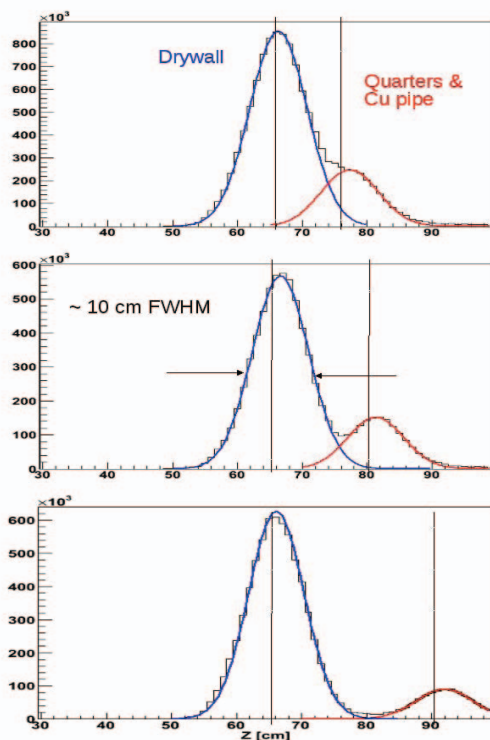


Fig. 4. 2-D images of a copper pipe and a stack of quarters at different Z positions. Two objects are 4cm apart in all cases while their Z positions are varied; 75cm (top), 80cm (middle), and 90cm (bottom) from the source. A drywall barrier was set up at 65cm from the source hiding the objects. Dotted lines show actual positions of the objects.